UNITED NATIONS EDUCATIONAL, SCIENTIFIC AND CULTURAL ORGANIZATION
INTERNATIONAL ATOMIC ENERGY AGENCY
INTERNATIONAL CENTRE FOR THEORETICAL PHYSICS
I.C.T.P., P.O. BOX 586, 34100 TRIESTE, ITALY, CABLE: CENTRATOM TRIESTE

H4.SMR/1013-19

SCHOOL ON THE USE OF SYNCHROTRON RADIATION
IN SCIENCE AND TECHNOLOGY:
"John Fuggle Memorial"

3 November - 5 December 1997

Miramare - Trieste, Italy

Coherent and incoherent processes in resonant photoemission

A. Nilsson
University of Uppsala
Sweden

Appl. Phys. A 65, 159–167 (1997)

Applied Physics A Materials Science & Processing

Coherent and incoherent processes in resonant photoemission

N. Mårtensson[1], M. Weinelt[1], O. Karis[1], M. Magnuson[1], N. Wassdahl[1], A. Nilsson[1], J. Stöhr[2], M. Samant[2]

[1] Department of Physics, Uppsala University, Box 530, S 751 21 Uppsala, Sweden
[2] IBM Research Division, Almaden Research Center, 650 Harry Road, San Jose, CA 95120, USA

Received: 6 March 1997

Abstract. The basis for resonant photoemission is discussed in connection with data for a physisorption system, Ar/Pt(111) and a $3d$ transition metal, Ni(100). For Ar/Pt(111) the quasi-localized character of the intermediate state leads to two types of features in the autoionization spectra, showing resonant Raman and normal Auger-like behaviour, respectively. For Ni(100) resonant Raman behaviour is observed in photoemission below the L_3 threshold. At threshold, the emission feature changes character and after a rather narrow transition region it appears at constant emission energy instead. Clear signatures of interference between the direct photoemission and autoionization channels are identified.

The properties of a system are determined by the valence electron distribution. The valence electrons occupy delocalized states which in a periodic solid correspond to the band structure of the system. These states can be probed by various valence electron spectroscopies such as photoemission, inverse photoemission or optical spectroscopy. However, the core levels also play important roles in the electronic structure. Furthermore, many experimental techniques which are used to study the electronic structure make use of the properties of the core electrons. In contrast to the valence electrons, the core electrons are localized to individual atoms in the system. This property can be used to highlight local aspects of the structure as well as the electronic structure. In XPS (X-ray photoelectron spectroscopy) the chemical shifts give information about the charge state, the chemical environment or even the cohesive properties of the core ionized site [1], shake-up features reflect the local electronic structure [2], the angular pattern of the emitted photoelectrons reflect the relative positions of the neighbouring atoms through diffraction effects [3], etc. In XAS (X-ray absorption spectroscopy) and XES (X-ray emission spectroscopy) unoccupied and occupied electron states can be probed. In XAS core electrons are promoted to empty valence electron states, while in XES a core vacancy is filled by a valence electron from an occupied orbital leading to the emission of a photon. These spectroscopies give site specific information and, furthermore, due to the fact that the transitions are dominated by dipole matrix elements the electronic structure information obtained is symmetry projected. In Auger electron spectroscopy one studies the deexcitation of core vacancies by electron emission processes.

The site-specificity of a core-level probe can also be achieved in valence electron spectroscopies by performing resonant measurements at core-level thresholds. The utilization of resonance effects provides most powerful ways to study the electronic structure of atomic, molecular and solid state systems [4–6]. Such techniques can be used to determine the atomic origin of valence electron states, to identify orbitals of different symmetries, to determine the symmetry of valence electron states and to study certain types of dynamic properties. In particular at the most modern storage rings the resonance effects can be used in a very powerful way. In order to obtain detailed information on the valence electron states the measurements have to be performed at high resolution. Furthermore, many of the most useful core-levels have rather high energies, often in the range of 500–1000 eV. It is only most recently that the necessary combination of resolution and flux has been achieved at these energies.

In resonant photoemission there is an interplay between direct photoemission and processes involving virtual excitations of intermediate core excited states which create the same final state when decaying by Auger-like (autoionization) processes [4–7]. In resonant inelastic X-ray scattering (RIXS) the corresponding virtual state decays by the emission of a photon, and we observe resonance effects in the inelastic scattering instead [8–12]. In the latter situation especially the total process is governed by very strict symmetry selection rules which may be used to establish the symmetry properties of the states involved. In the present contribution we will discuss general aspects of resonant phenomena based on investigations of resonant photoemission.

International Workshop "Resonant Inelastic Soft X-ray Scattering (RIXS)", Walberberg, 5–7 September 1996

The term resonant photoemission is used in somewhat different ways based on more or less strict requirements on the process. Primarily we mean that the intensity of a photoemission feature is affected when the photon energy is varied over a core-level threshold. Usually this corresponds to an intensity enhancement but in certain cases the resonance effects can also lead to other types of intensity modifications. It may even happen that the core-level process produces a reduction of the intensity [13].

In solid systems it is not sufficient to base the criteria on the intensity variations alone.The core-level binding energy also defines the onset of regular Auger processes. These may then be enhanced as a consequence of the large absorption cross-section at the XAS white line. It is therefore necessary to be able to distinguish between those autoionization processes which produce photoemission-like features and those which behave like regular Auger processes. When the measurements are performed at sufficiently high resolution one can in many cases make this distinction. This is done first of all by carefully studying the energy of the emission features as the photon energy is swept in small steps over the absorption profile. For the process to be photoemission-like it is necessary that the kinetic energy of the spectral features disperse linearly with photon energy. The phenomenon of linear dispersion for autoionization features is often referred to as the resonant Raman effect [10]. This is different from the situation for regular Auger processes which involve the decay of well-defined (lifetime broadened) states of given energy, leading to emission energies which are independent of the excitation energy. However, at threshold there may be energy tracing effects also in processes which one would denote 'Auger-like' [6, 24].

The third and strictest condition for resonant photoemission is that there is interference between the direct and the core-hole assisted processes. This implies that the intensity is not simply a sum of the intensities of the individual subprocesses. The interference leads to Fano-like profiles for the intensity as a function of photon energy [6, 13, 14]. Sometimes, the term resonant photoemission is used only when clear signatures of interference are seen. However, as will be seen below this may be misleading. If interference effects are observed the process is indeed resonant. On the other hand, the absence of observable interference effects may be due either to the fact that there is no interference or to the fact that the interference terms happen to be very small due to the dominance of a single channel.

In the present contribution we will discuss the distinction between coherent and incoherent processes in resonant photoemission. As a first step we discuss what determines whether an autoionization process is photoemission-like or Auger-like. The discussion is based on measurements for a weakly bonded adsorption system, Ar/Pt(111) [15]. This type of system is well adapted to investigating these effects since it yields distinctly shifted spectral features depending on the nature of the process. After this the question of resonant photoemission in metallic systems is addressed. This is done in connection with measurements at the $2p$ edges for Ni metal. Ni has been one of the prototype systems for resonant photoemission. The resonances have been discussed in connection with the strong correlation and d-band localization effects in this system. Based on the results some general comments about the appearance of resonant effects in metallic systems are made.

1 Experimental

The experiments were performed using beamline 8.0 at the Advanced Light Source.This undulator beam line is equipped with a modified 'Dragon' monochromator with a resolving power of up to 10^4. The end-station was built at Uppsala University and comprises two rotatable spectrometers, a Scienta SES200 electron spectrometer [16] and a high-resolution grazing incidence grating spectrometer for X-ray fluorescence studies [17]. In the Ar measurements the resolution was set to 100 meV for the monochromator and to 200 meV for the spectrometer. In the Ni measurements the resolution was 100 eV in both channels. The spectra for Ar/Pt(111) were measured at low temperatures using a liquid He flow cryostat.

2 Character of the autoionization process

The Auger process is normally described as a two-step process. In the first step a photoelectron is emitted from a core orbital. In the second step the core vacancy is filled by a less tightly bound electron and an additional electron, the Auger electron, is emitted. The energy of the Auger electron is given by the difference in total energy between the initial core vacancy state and the final two-hole state. Due to the finite lifetime of the core-hole state the energy of the photoelectron has an uncertainty leading to a Lorentzian broadening of the photoelectron line. This is also manifested as a corresponding broadening of the Auger transition. However, if the photoelectrons and Auger electrons could be measured in coincidence the sum of the kinetic energies of the two electrons would be independent of the core-level width. The intrinsic broadening of the summed energies would only be due to the lifetime of the final two-hole state. If one could set one of the analysers in a coincidence experiment to a fixed narrow energy window at the photoelectron peak position the measured coincidence Auger spectrum would not be influenced by the core-level width. Furthermore, if in this experiment one could increase the photon energy slightly but in such a way that the photoelectron analyser still covers part of the photoelectron line one would observe the same Auger spectrum but with a corresponding kinetic energy shift.

With synchrotron radiation one can also study the Auger decay following resonant excitation of a neutral core excited state (XAS final state). This process is called resonant Auger decay or autoionization. In this process only one electron is emitted and the final state is singly charged. When performing resonant Auger measurements with photon energy bandwidths smaller than the core-hole linewidth the Auger resonant Raman effect has been identified [10, 18, 19]. This implies that the resonant Auger transitions can have linewidths which are smaller than the lifetime broadening of the core hole state. Furthermore, within the width of an individual absorption resonance the resonant Auger line disperses linearly with photon energy. This implies that the resonant Auger process has to be described as a single quantum mechanical process with energy conservation criteria like in normal photoemission. This may also be discussed in terms of coherence between the excitation and deexcitation steps [20–23].

This type of coherence is a necessary requirement for resonant photoemission. The distinction between coherent and incoherent processes is therefore important for the basic un-

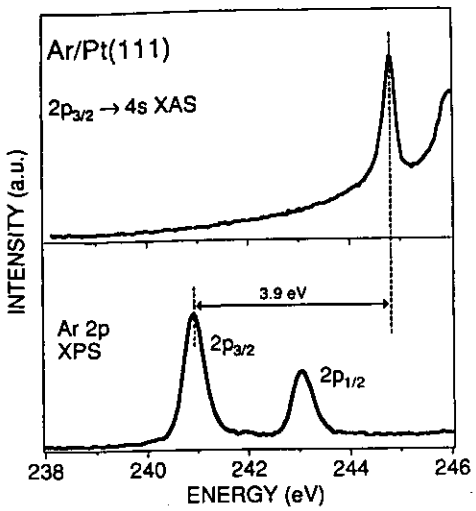

Fig. 1. The Ar $2p_{3/2} \rightarrow 4s$ XA and the Ar $2p$ XP spectra shown on a common energy scale for Ar/Pt(111). For XPS the binding energy is given relative to the Fermi level. For XAS the photon energy is used

derstanding of resonant photoemission and has recently been investigated for a couple of prototype systems [15,25]. We show how the coherence is influenced by the core excited state in connection with autoionization spectra from the system Ar/Pt(111) [15]. This is an interesting system since there is only weak interaction between the adsorbed Ar atoms and the substrate. In fact, if we define the interaction strength in terms of a characteristic hopping time for an electron between the adsorbate and the substrate, we find that this time is very similar to the lifetime of the core excited state. This implies that the decay spectra will be very sensitive to the localization–delocalization properties of the core excited state.

In Fig. 1 the Ar $2p_{3/2} \rightarrow 4s$ XA and $2p$ XP spectra are shown. The spectra are plotted on a common energy scale. In the case of XPS the energy scale corresponds to the binding energy relative to the Fermi level whereas for XAS the normal photon energy scale is used. In this way the total energy of the created final states can be directly compared. As can be seen the energy of the $2p_{3/2}$ ionic final state is 3.9 eV lower than the energy of the main XAS final state. The resonance in XAS is due to excitations to the $4s$ level of Ar. However, it is evident from the spectral shape that the atomic $4s$ level is modified by the interaction with the substrate [26]. The feature is broadened and it has a tail extending all the way down to the energy of the Ar $2p_{3/2}$ XPS peak. This implies that the states to which the core electron is promoted are due to $4s$-substrate hybride states. Due to the dominant atomic character we may view the resonance states as quasi-localized $4s$ derived atomic states. We will discuss in more detail below how the properties of these states vary over the resonance.

Figure 2 shows electron emission (autoionization) spectra for a number of photon energies around the XAS resonance. The overall spectral shape changes with the photon energy. Two sets of spectral features can be identified, one which stays at constant kinetic energy and one which moves with the photon energy. The shapes of the two parts of the spectra seem to be independent of the excitation energy. The relative weights of the two parts, however, vary.

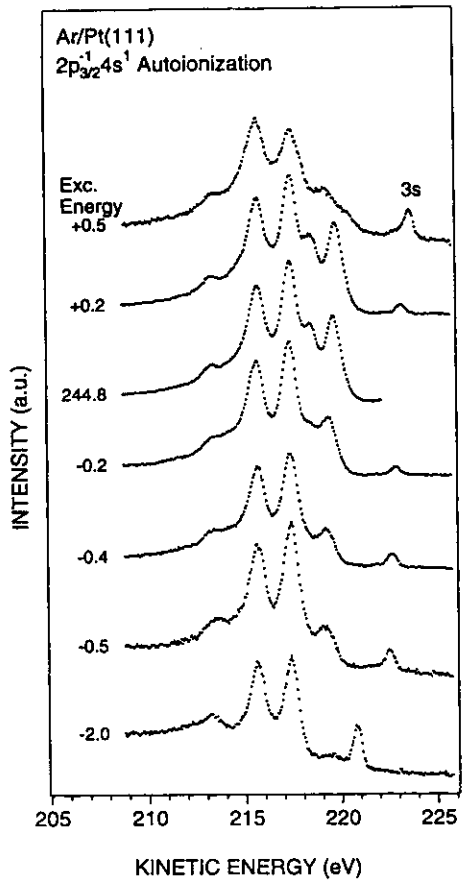

Fig. 2. Ar/Pt(111) autoionization spectra for several photon energies around the $2p_{3/2} - 4s$ resonance

Figure 3 shows an analysis of the spectrum recorded at the resonance maximum (244.8 eV). The spectrum can be accurately reproduced by a summation of two model spectra. The curve denoted by (+) corresponds to a $2p_{3/2}$ Auger spectrum recorded for the Ar/Pt sample using a photon energy well above the XAS resonance. The different peaks in the

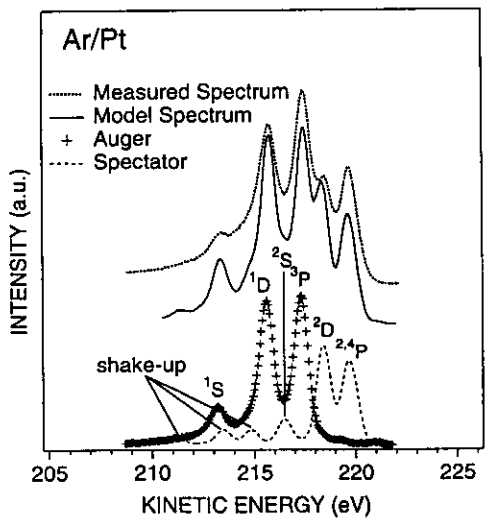

Fig. 3. A fit of the autoionization spectrum for an excitation energy at the resonance maximum, see text

spectrum are due to the multiplet levels of the $3p^4$ final state configuration as denoted in the figure. The dashed curve is a gas phase autoionization spectrum following the excitation of the $2p_{3/2}^{-1}4s^1$ state. The identification of the peaks is given in the figure. The spectrum has been convoluted with a Gaussian of width 0.3 eV and shifted to achieve the best possible fit. By summing these spectra with appropriate weight factors we obtain the model spectrum given by the solid line. As can be seen this curve mimics all essential features of the experimental Ar/Pt autoionization spectrum. The remaining small differences appear mainly in the shake-up part of the autoionization spectrum [27, 28]. This is due to the interaction of the Ar orbitals with the substrate which modifies especially the extended orbitals involved in the shake-up processes. There may also be slight differences in the remaining parts of the spectra caused by small modifications of the splittings and relative intensities of the multiplet components. Similar decompositions have been performed for the decay spectra over the entire $4s$ resonance profile, giving the same type of agreement. Each spectrum may thus be thought of as consisting of two parts, one with an Auger-like $3p^{-2}$ final state and one with a $3p^{-2}4s^1$ spectator-like final state [15, 26].

Figure 4 displays the kinetic energy of the two sets of spectral features. As can be seen the $3p^{-2}$ features stay at constant kinetic energy while the kinetic energy of the $3p^{-2}4s$ features increases with photon energy. The measured position follows very closely the dashed line which corresponds to constant binding energy; it shows resonant Raman behaviour. Hence the two types of spectral features can be characterized as constant binding energy and constant kinetic energy features, respectively. In the final state of the constant binding energy process the excited electron appears in an atomic-like Ar $4s$ orbital. In the final state of the constant kinetic energy process the excited electron is instead located in the substrate. The final state is a doubly charged Ar^{++} ion. Both final states are screened by polarization of the substrate (image charge screening).

The state at constant binding energy may be viewed as a resonantly enhanced photoemission-like final state with energy conservation in terms of the normal type of photoemission relation, $E_{kin} = h\nu - E_B$ $(3p^{-2}4s^1)$. This implies that the excitation and deexcitation steps cannot be separated. The spectral behaviour has to be described in a one-step scattering picture and the intensity is given by the following type of expression [6]:

$$w = 2\pi \sum_f \left| \sum_m \frac{\langle f|V_A|m\rangle\langle m|V_r|g\rangle}{E_g - E_m - \frac{i\cdot\Gamma_m}{2}} \right|^2 \cdot \delta(E_f - E_g) . \qquad (1)$$

In this formulation the initial (g) and final (f) state wave functions contain the incoming photon and the outgoing electron, respectively, and (m) denotes the intermediate states. V_r and V_A denote the radiative and Coulomb (Auger) contributions to the interaction, respectively, and Γ_m is the lifetime width of the core excited state. The delta-function ensures energy conservation.

The constant kinetic energy feature can also be viewed in terms of an autoionization process. In this case the spectator electron in the final state occupies a state which is entirely located in the substrate. The fact that we observe a constant kinetic energy feature implies that the energy released in the core-hole decay is independent of the energy of the spectator electron. The energy of the final state may be viewed as the sum of two terms, the energy of the (polarization screened) two-hole final state of the adsorbate and the energy of the spectator electron (relative to the Fermi level) in the substrate. When the excitation energy is varied this only changes the energy of the spectator electron and the features in the decay spectra remain at the same kinetic energies. The energy of the spectator electron never appears in the spectrum. The presence of this additional excitation thus prevents energy conservation for those particles which we observe in the decay. In this case the width of the autoionization features will also be influenced by the core-hole lifetime. The lifetime broadening will give an uncertainty of the energy of the spectator electron and a corresponding uncertainty for the Auger electron. The result of this is that the measured Auger-like spectrum will contain features which are broadened due to the finite lifetime of the core-hole state. All the important features of the spectra are thus as expected for a two-step process in which the memory of the excitation is lost. In a strict sense also this process is a one-step process. However, in a one-step treatment one would have to integrate the emission probabilities over all final states which lead to the same energy of the emitted electrons. This integration would essentially only lead to a broadening of the spectral features due to the finite lifetime of the core excited state. The spectrum will thus be identical to the spectrum obtained in a two-step description where the core-level broadening is introduced by a simple convolution.

The distinction between a one-step and a two-step process is thus mainly a practical distinction. If all particles in the process are detected a one-step description is necessary. If, on the other hand, there are excitations (particles or quasi-particles) which are not detected in the process, the information is incomplete. It may then be sufficient to describe the process in a two-step picture. In this case the core-hole state will have a profile which has to be considered in the calculation. Unless coincidence techniques are used this implies that the distinction between one- and two-step processes corresponds

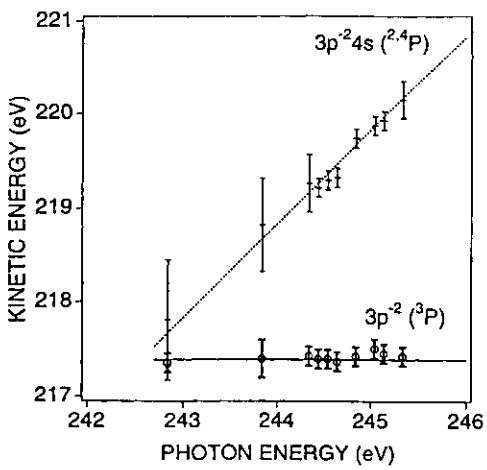

Fig. 4. The kinetic energies of the $3p^{-2}(^3P)$ and the $3p^{-2}(^3P)4s^1$ lines are plotted for different excitation energies around the $2p_{3/2} - 4s$ resonance for Ar/Pt(111). The dotted line corresponds to constant binding energy

to a distinction between two-particle processes and processes involving three or more particles (quasi-particles) [15, 29].

The detailed appearance of the autoionization spectra depends on the properties of the intermediate state. If the excited $4s$ electron were purely atomic there would only be $3p^{-2}4s^1$ final state features in the spectra. The presence of $3p^{-2}$ states in the decay spectra is thus a consequence of the fractional occupancy of the $4s$ orbital due to mixing with the substrate orbitals. We may view the process in terms of a '$4s$' wave-packet set up at the Ar site. Due to the interaction with the substrate this wave-packet will have some substrate character as well. Furthermore, the wave-packet will continue to delocalize on the time scale of the core-hole decay. Both these effects depend on the degree of localization of the intermediate states involved. In a time-dependent picture the fraction of final states of each type is then given by the '$4s$' weight at the time of the decay.

By scanning the excitation energy over the $4s$ resonance we may investigate the effects of changing the character of the intermediate state wave-function. The $4s$ character is largest at the centre of the resonance and the substrate contribution increases as one approaches the flanks. In Fig. 2 we observe that both types of features are present in all the spectra but that the relative intensities change with excitation energy.

Figure 5 displays the relative weight of the $3p^{-2}4s^1$ final state feature for different photon energies over the $4s$ resonance. We call this the coherent fraction in accordance with the discussion above. As can be seen this fraction is largest at the resonance position where the $4s$ character is largest and tails off away from the resonance maximum. In particular, for excitation energies close to threshold this fraction is very small. From this it is clear that the intensity of the photoemission-like features depends critically on the degree of localization of the intermediate state.

The probability of creating $3p^{-2}4s^1$ final state features by direct photoemission is very small since this corresponds to a shake-up process. This process is so weak that for all practical purposes it can be neglected at resonance. It is therefore not possible to observe any interference effects between the autoionization and the direct photoemission channels.

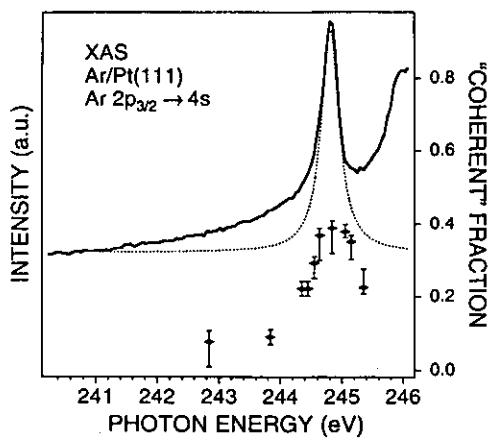

Fig. 5. The relative intensity of the decay to the $3p^{-2}4s^1$ final state for excitation energies around the $2p_{3/2}4s$ resonance for Ar/Pt(111). We call this the coherent fraction. The error bars are obtained from the variations of the parameters in the decomposition of the autoionization spectra

3 Interference effects in Ni

In order to investigate the possibility of interference effects we turn to Ni metal as a sample. Ni has been one of the prototype systems for resonant photoemission. Guillot et al. [4] observed at the $3p$ core-level threshold a strong enhancement of a valence band satellite which occurs at 6 eV binding energy. This satellite has been interpreted as due to a localized $3d^8$ final state [30]. The resonance was described in terms of a virtual process involving the excitation of a $3p$ electron to the partly unoccupied $3d$ shell followed by an Auger-like decay leading to a $3d$ double-hole state. The same type of final state is the dominating one in the normal Auger decay in Ni. The interpretation of the Ni results in terms of resonant photoemission has, however, been challenged in recent years [20–23]. It has been argued that the core excited intermediate states are not localized enough to allow the resonant processes to occur. It has been proposed instead that the resonantly enhanced photoemission satellite in Ni is due to incoherent Auger processes which are enhanced at the same photon energies due to the strong absorption just above the core edge [21, 22]. Due to the complete metallic screening the Auger-like and photoemission-like spectral features cannot be distinguished in the same straightforward way as in the Ar/Pt(111) system. At threshold the two types of processes will in fact give spectral features at more or less identical energies. In order to determine whether there is resonant photoemission in Ni or not it is therefore necessary to find out in some other way if the process is photoemission-like or not. One way to do this is to investigate if there are any signatures of interference between the direct photoemission and the core-hole assisted processes.

In the case of resonant photoemission the intensity in (1) will also contain a direct photoemission term [6]:

$$w = 2\pi \sum_f \left| \langle f|V_r|g\rangle + \sum_m \frac{\langle f|V_A|m\rangle\langle m|V_r|g\rangle}{E_g - E_m - \frac{i\cdot\Gamma_m}{2}} \right|^2 \cdot \delta(E_f - E_g) . \qquad (2)$$

For each final state the intensity is thus given by a sum of a direct photoemission term and a set of terms describing the core-hole assisted (autoionization) processes.

The expression can be reformulated as a sum of intensities of the separated photoemission and autoionization processes plus an interference term. Under certain conditions a standard Fano cross-section, $I \approx (q+\epsilon)^2/(\epsilon^2+1)$ is obtained, where $\epsilon = (E - E_{th})/\Gamma$ [6]. The shape of the Fano profile is determined by the asymmetry parameter q. The square of this parameter is proportional to the ratio between the strengths of the core level assisted (autoionization) process and the strength of the direct photoemission continuum over the core-hole width. Usually the interference leads to reduced transition rates below threshold and enhanced intensities above. A set of Fano profiles with values of q ranging from 0 to 3 is shown in Fig. 6. A large q ($q \gg 1$) corresponds to a Lorentzian-like enhancement. With decreasing q the line profile gets more asymmetric and $q = 1$ gives an asymmetric Fano-profile with a minimum at $\epsilon = -1$ and an equally large maximum at $\epsilon = 1$. As seen from the figure $q = 0$ gives a dip in the photoionization continuum.

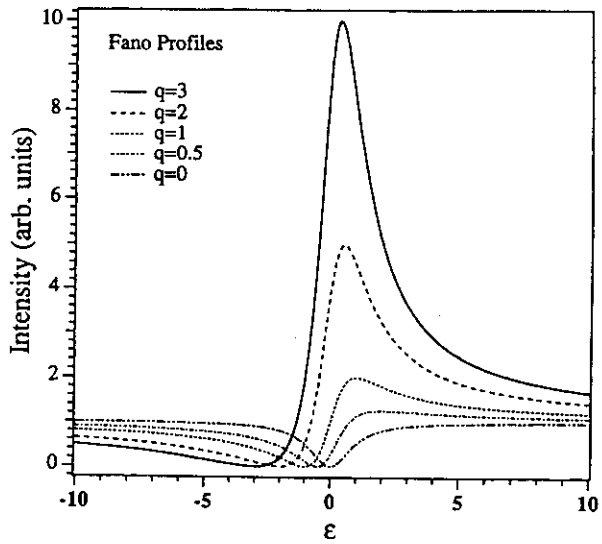

Fig. 6. A schematic illustration of line profiles of a Fano resonance (see text) for different values of the q-parameter

We have performed photoemission measurements for the valence electron region at the $2p$ edges of Ni. The $2p$ edges give better possibilities studying the resonance effects than the shallow $3p$ edges. One difference is that the $2p$ levels are narrower. More importantly, the large $2p$ spin–orbit splitting gives well-separated $2p_{1/2}$ and $2p_{3/2}$ resonances instead of the overlapping $3p_{1/3,3/2}$ resonances. The fact that the $2p$ resonances occur at higher photon energies also has the advantage that there are fewer additional photon energy dependent effects. Such effects may be due to varying photoemission matrix elements and effects of crystal momentum selectivity (k-conserving transitions).

Figure 7 compares a set of valence electron spectra recorded for photon energies up to the L_3 absorption threshold at 852.3 eV. The spectra are shown on a kinetic energy scale. The dashed and solid curves correspond to measurements with the E-vector in the plane of the surface and parallel to the surface normal, respectively. We have used a unique experimental set-up which allows the E-vector of the photon beam to be varied without changing at the same time the direction of the emitted photoelectrons relative to the sample. This is achieved by rotating simultaneously the sample and the spectrometer around an axis along the direction of the incoming beam. Starting with the spectra well below resonance we see two types of states; band-like states within ≈ 2.3 eV from the Fermi level which dominate the spectra and split-off atomic-like $3d^8$ satellite states at 6 eV. The intensities of both spectral features are much larger for the E-vector out of the plane. We therefore call this the 'photoemission geometry'. When approaching the L_3 resonance position, the relative weight of the satellite increases. At resonance, both contributions and in particular the satellite are much enhanced and furthermore the intensity is now the same for both experimental geometries. Above resonance the normal photoemission spectrum which was seen below resonance reappears but is not shown here. In addition there is a feature which stays at the same kinetic energy as was obtained for the satellite at resonance. This is due to the normal Auger decay of the $2p_{3/2}$ vacancy states. As can be seen the Auger intensity is essentially the same for the two experimental geometries (the small difference in Fig. 7 is probably due to problems in normalizing the spectra at different polarizations relative to each other). Since the Auger intensity is the same for the two geometries we call the one in which the photoemission intensity has a minimum the 'Auger geometry'.

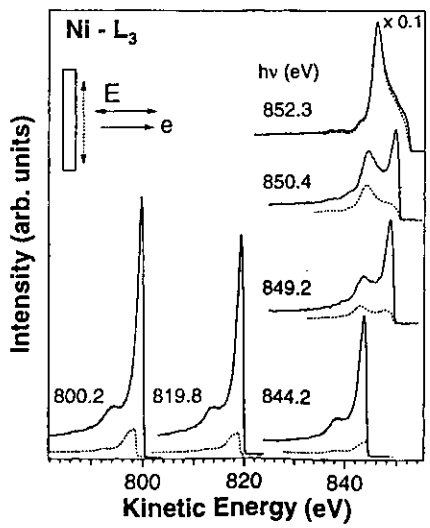

Fig. 7. Valence electron spectra (on a kinetic energy scale relative to the Fermi level) recorded around the Ni L_3 threshold. The E-vector of the incident X-rays is in the surface plane (dashed line) or perpendicular to it (solid line)

We have investigated the intensity of normal valence band emission as well as of the satellite. We denote the ground state in Ni as $[3d^9 4s]$ where the square brackets indicate that the valence electrons are in the metallic state. The final state in the normal valence band photoemission process can be written as $[3d^9 4s]^{-1}$. The valence band hole in this state is delocalized. Taking screening into account the satellite state may be written as $3d^8(X)[4s^2]$ (X is a spectroscopic assignment of the atomic $3d^8$-configuration). The screening electron is taken from the Fermi level. The same type of final states can be reached at the $2p$ threshold due to the excitation of an intermediate $2p^{-1}[3d^{10}4s]$ state. This state may decay by electron emission in an Auger-like process (autoionization). Normal Auger in Ni is known to lead to localized as well as delocalized final states of the above type [26].

Figure 8 shows in more detail spectra recorded for photon energies around the $2p_{3/2}$ core level threshold in the photoemission geometry. In this case the spectra are plotted on a binding energy scale. Below threshold, the whole spectrum stays at constant binding energy and the intensities of the different parts of the spectra change as discussed above. Immediately above threshold, we observe how the 6 eV feature starts to move to higher binding energies as the photon energy increases. This immediately shows that final states are produced which are not identical to the photoemission final states. This is completely analogous to the situation with the appearance of Auger-like features in Ar/Pt(111) as discussed above. We can also discuss this as a loss of coherence in the process [15]. There are excitations in the system which we do not detect. Also in the valence band region we observe how a weak shoulder develops from the Fermi-level cut-off and starts to disperse with photon energy. This demonstrates the appearance of Auger-type features in the band-like part of the spectrum.

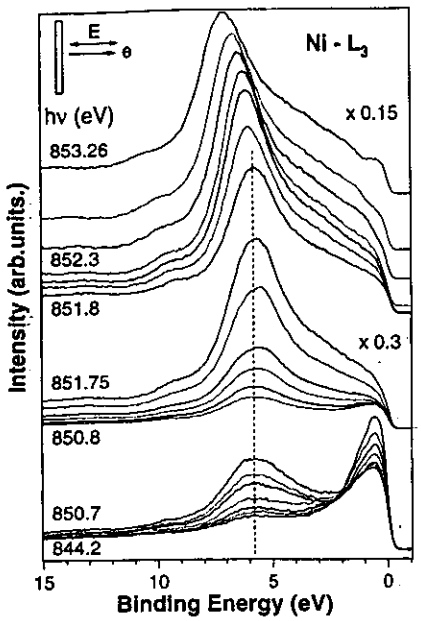

Fig. 8. Valence electron spectra around the L_3 core level threshold on a binding energy scale. The spectra have been measured in the 'photoemission geometry'. The photon energy increment is about 0.2 eV except for the lower set of data (844.2, 848.0, 849.0, 849.8, 850.3, 850.5 and 850.7 eV)

The kinetic energy (peak position) of the $3d^8[4s^2]$ spectral feature is plotted in Fig. 9 as a function of photon energy for the 'photoemission' and for the 'Auger' geometries. Below the $2p_{3/2}$ resonance maximum the kinetic energy tracks perfectly the photon energy (resonant Raman behaviour). At threshold, the peak transforms rapidly into a constant kinetic energy feature. There is only a narrow transition region in which the energy positions deviate slightly from the two straight lines. There are a number of effects which can give this type of deviation in a narrow energy range. There may be multiplet-like effects and there may be apparent shifts due to the finite energy spread of the photon beam [19]. However, it seems that at least part of the deviation from the

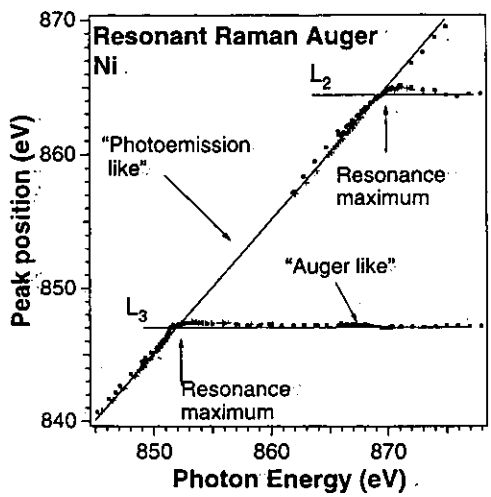

Fig. 9. The energy of the $3d^8[4s^2]$ spectral feature as a function of photon energy

pure Auger-like behaviour above the $2p_{3/2}$ edge is due to a photoemission component which is resonantly enhanced as well. The behaviour has been investigated also at the $2p_{1/2}$ threshold yielding very similar results (not shown here).

The photon energy dependence shows that the process below threshold is photoemission-like. This is the case all the way up to photon energies very close to threshold. Immediately above threshold most of the intensity becomes incoherent. From the spectra we cannot with confidence identity any resonantly enhance coherent intensity in this regime. This implies that if we integrate over the whole photon energy range at which the resonance appears a large fraction of the enhanced intensity is indeed incoherent. In order to determine whether there is resonant photoemission in Ni we therefore have to turn to the detailed intensity profiles in order to check directly for signatures of interference.

In order to probe the character of the resonant process we follow the photon energy dependence of the intensity for a region in the valence band spectrum close to the Fermi level and for an energy window around the 6 eV satellite (see Fig. 10). This has been done both for the 'Auger' and for the 'photoemission' geometries. The two top curves show the valence band intensity in the 'photoemission' (top) and 'Auger' (middle) geometries. It is immediately seen that the intensities show characteristic Fano-like profiles. At the bottom the results for the 6 eV satellite are shown. The curves for the 'Auger' and 'photoemission' geometries are plotted together. Looking at the individual curves there is no clear indication of a resonance line shape. However, when comparing the measurements for the two geometries (see inset) differences in the profiles are observed which are characteristic of Fano profiles with different q. This shows immediately that there are inter-

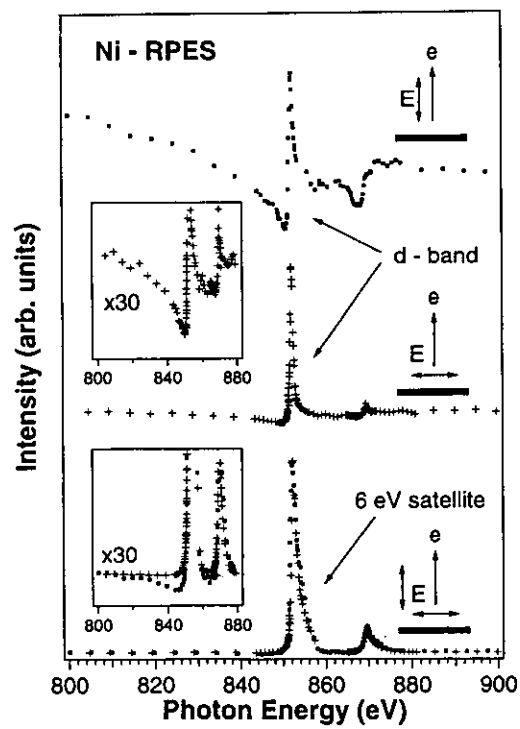

Fig. 10. Intensity of the valence-band emission (top two curves) and the 6 eV satellite (bottom set of curves, plotted together) as function of photon energy in the 'photoemission' and 'Auger geometries'

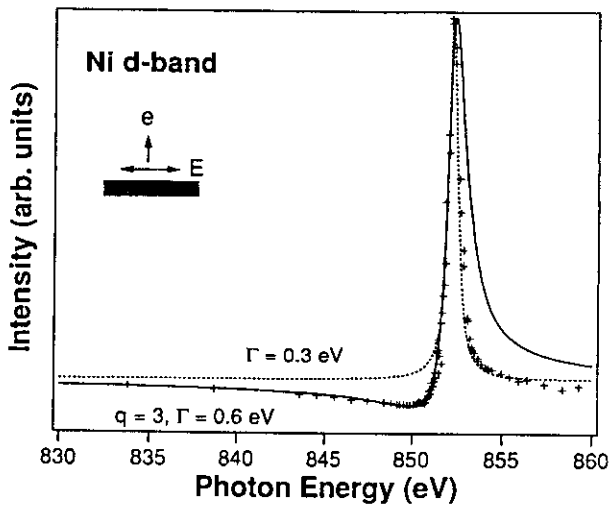

Fig. 11. A Fano profile and a Lorentzian fitted to the experimental photon energy dependence of the valence band intensity recorded in the 'Auger geometry'

ference effects also in these spectra. The interference term is small but this is due to the fact that the autoionization channel is dominating so strongly. This demonstrates that the absence of visible interference effects is not a good criterion for the absence of interference. This may instead be due to the total dominance of one of the spectroscopic channels.

We find that the curves cannot be fitted with standard Fano line shapes. One reason for this is that the core excited states change character above threshold (delocalization of the intermediate state). We have a situation with several discrete states and several continua. This is different from the basic assumptions for the Fano-model, i.e. a discrete state and an underlying continuum. In spite of this it may be instructive to compare the profiles to the Fano model in order to get an approximate measure of the importance of the interference in terms of a single parameter, the Fano asymmetry parameter q. An example of such a 'fit' is seen in Fig. 11 for the valence band emission in the 'Auger' geometry. Fitting mainly the first part of the resonance profile we obtain a value of $q = 3$ for the asymmetry parameter. However, this fit gives a lifetime width of 0.6 eV which makes the resonance peak much too wide. If the profile is fitted with a symmetric Lorentzian the broadening is reduced to 0.3 eV. This demonstrates the fact that single Fano profiles do not give good descriptions of the resonances. We will anyway use the obtained q-values to give an approximate idea about the trends of the q-values in different situations.

Comparing the intensity profiles in Fig. 10 to the model Fano profiles in Fig. 6 it is evident that q is smallest for the valence band, in particular in the 'photoemission' geometry ($q \approx 1.5$ at the $2p_{3/2}$ resonance). This channel is the majority channel in photoemission and the minority one in autoionization, yielding similar magnitudes of the matrix elements in (2). For the satellite, the opposite situation is true and consequently much larger q-values are found ($q > 20$ and $q \approx 9$ in the 'Auger' and 'photoemission' geometries, respectively). Going to the $2p_{1/2}$ edge, we find in all cases more pronounced Fano-like profiles corresponding to smaller q-values (e.g. $q \approx 0.5$ for the valence band in the 'photoemission' geometry) as expected due to the weaker absorption and larger lifetime width of the L_2 level (see the definition of q above). The trends are fully consistent with the expectations from the Fano model and we therefore conclude that the shapes of the resonance profiles are due to interference.

4 Summary and conclusions

We have investigated the basis for resonant photoemission for two prototype systems, one weakly bonded adsorption system and one transition metal. We find that for Ar/Pt(111) there are two types of features in the spectator autoionization spectra. One of these shows resonant Raman behaviour and has to be treated in a one-step picture. The other one shows normal Auger-like behaviour and can be described in a two-step picture. This branching is due to the quasi-localized character of the intermediate state. The intermediate state is localized enough to yield a constant binding energy feature for excitation energies over the entire resonance, although of varying relative strength. The Auger-like feature dominates at most energies and corresponds to final states in which the spectator electron is located in the substrate. The spectator electron may have a distribution of energies and the scattering process can be viewed as the creation of two particles which share energy. Since we observe only one of these we recognize this as a loss of coherence and as an apparent loss of conservation of energy.

We have also performed measurements of the resonant photoemission for a Ni(100) sample with special emphasis on the possible interference between the autoionization and the direct photoemission channels. We observe clear signatures of interference both for the main valence band emission and for the 6 eV satellite. The spectra show resonantly enhanced photoemission-like spectral features only in the region before threshold. We call this the resonant Raman regime. For photon energies above threshold the emission features rapidly transform into features which appear at constant kinetic energy. In terms of the possible interference with the direct photoemission process this corresponds to a loss of coherence. This implies furthermore that a large fraction of the totally observed resonantly enhanced intensity is incoherent. The results indicate that the resonance behaviour is not explained by any strongly localized intermediate state in the resonant scattering process. This also implies that resonance phenomena and especially the interference effects may occur also in systems with very delocalized excited states.

Acknowledgements. This work was supported by the Swedish Natural Science Research Council (NFR), the Göran Gustavsson Foundation for Research in Natural Sciences and Medicine and the Swedish Institute (SI). ALS is supported by the US Department of Energy, under contract No. DE-AC03-765F00098.

References

1. B. Johansson, N. Mårtensson: Phys. Rev. B **21**, 4427 (1980)
2. N. Mårtensson, A. Nilsson: Applications in Synchrotron Radiation, Springer-Verlag, Berlin, Germany, p. 65–126 (1995)
3. C.S. Fadley: Surf. Sci. Rep. **19**, 231 (1993)
4. C. Guillot, Y. Ballu, J. Paigné, J. Lecante, K.P. Jain, P. Thiry, R. Pinchaux, Y. Pétroff, L.M. Falicov: Phys. Rev. Lett. **39**, 1632 (1977)
5. L.C. Davis, L.A. Feldkamp: Phys. Rev. B **23**, 6239 (1981)

6. C.-O. Almbladh, L. Hedin, in Handbook on Synchrotron Radiation E.-E. Koch, eds. (North-Holland Publishing Company, Amsterdam, New York, Oxford, 1983), vol. 1B, pp. 607
7. G. Wedin: Comments At. Mol. Phys. **17**, 115 (1986)
8. Y. Ma: Phys. Rev. B **49**, 5799 (1994)
9. F. Gel'mukhanov, H. Ågren: Phys. Rev. A **49**, 4378 (1994)
10. T. Åberg, B. Crasemann: in Resonant Anomalous X-ray scattering G. Materlik, C.J. Sparks, K. Fischer, Eds. (Elsevier Science B.V., Amsterdam, 1994) pp.430
11. Y. Ma, K.E. Miyano, P.L. Cowan, Y. Aglitzkiy, B.H. Karlin: Phys. Rev. Lett. **74**, 478 (1995)
12. J.A. Carlisle, E.L. Shirley, E.A. Hudson, L.J. Terminello, T.A. Callcott, J.J. Jia, D.L. Ederer, R.C.C. Perera, F.J. Himpsel: Phys. Rev. Lett. **74**, 1234 (1995)
13. U. Fano: Phys. Rev. **124**, 1866 (1961)
14. U. Fano, J.W. Cooper: Rev. Mod. Phys. **40**, 630 (1968)
15. O. Karis, A. Nilsson, M. Weinelt, T. Wiell, C. Puglia, N. Wassdahl, N. Mårtensson, M. Samant, J. Stöhr: Phys. Rev. Lett. **76**, 1380 (1996)
16. N. Mårtensson, P. Baltzer, P. Brühwiler, J.-O. Forsell, A. Nilsson, A. Stenborg, B. Wannberg: J. Electron Spectrosc. Rel. Phenom. **70**, 117 (1994)
17. J. Nordgren, R. Nyholm: Nud. Instrum. Methods A **246**, 242 (1986)
18. O.S. Brown, Chen-Hsiung-Mau, B. Crasemann, G.E. Ice: Phys. Rev. Lett **45**, 1937 (1980)
19. A. Kiwimäki, A.N. de-Brito, S. Aksela, H. Aksela, O.P. Sairanen, A. Ausmees, S.J. Osborne, L.B. Dantas, S. Svensson: Phys. Rev. Lett **71**, 4307 (1993)
20. M.F. López, A. Höhr, C. Laubschat, M. Domke, G. Kaindl: Europhys. Lett. **20**, 357 (1992)
21. M.F. López, C. Laubschat, A. Gutiérrez, E. Weschke, A. Höhr, M. Domke, O. Kaindl: Surf. Sci. **307-309**, 907 (1994)
22. M.F. López, C. Laubschat, A. Gutiérrez, G. Kaindl: Z. Phys. B **94**, 1 (1994)
23. M.F. López, C. Laubschat, A. Gutiérrez, A. Höhr, M. Domke, G. Kaindl, M. Abbate: Z. Phys. B **95**, 9 (1994)
24. W. Drube, R. Treusch, G. Materlik: Phys. Rev. Lett. **74**, 42 (1995)
25. M. Weinelt, A. Nilsson, M. Magnuson, T. Wiell, N. Wassdahl, O. Karts, A. Föhlisch and N. Mårtensson: Phys. Rev. Lett. **78**, 967 (1997)
26. W. Wurth, G. Rocker, P. Feulner, R. Scheuerer, L. Zhu, D. Menzel: Phys. Rev. B **47**, 6697 (1993)
27. H. Pulkkinen, S. Aksela, O.P. Sairanen, A. Hiltunen, H. Aksela: J. Phys. B **29**, 3033 (1996)
28. A. Kikas, S.J. Osborne, A. Ausmees, S. Svensson, O.P. Sairanen, S. Aksela: J. Electr. Spec. **77**, 241 (1996)
29. E. Kukk, H. Aksela, S. Aksela, F. Gelmukhanov, H. Ågren, S. Svensson: Phys. Rev. Lett **76**, 3100 (1996)
30. S. Hüfner, G.K. Wertheim: Phys. Lett. **51A**, 299 and 301 (1975)
31. P.A. Bennett, J.C. Fuggle, F.U. Hillebrecht, A. Lenselink, O.A. Sawatzky: Phys. Rev. B **27**, 2194 (1983)